Carbohydrate Polymers 108 (2014) 206–215

Contents lists available at ScienceDirect

Carbohydrate Polymers

journal homepage: www.elsevier.com/locate/carbpol

Removal of metal ions from water using nanohydrogel tragacanth gum-g-polyamidoxime: Isotherm and kinetic study

Arameh Masoumi, Mousa Ghaemy*

Polymer Research Laboratory, Faculty of Chemistry, University of Mazandaran, Babolsar, Iran

ARTICLE INFO

Article history:
Received 9 November 2013
Received in revised form 18 February 2014
Accepted 24 February 2014
Available online 11 March 2014

Keywords:
Tragacanth gum
Graft copolymerization
Metal ion
Bioadsorbent
Isotherm
Kinetic

ABSTRACT

A new biosorbent was prepared by grafting polyacrylonitrile onto iranian tragacanth gum (ITG), a naturally and abundantly available polysaccharide, and subsequent amidoximation in the presence of hydroxylamine hydrochloride. This nanohydrogel with amidoxime functional groups [—C(NH_2)═NOH], named polyamidoxime-g-tragacanth (ITG-g-PAO), was characterized and used for the removal of metal ions from aqueous solution. The effect of pH, agitation time, concentration of adsorbate and amount of adsorbent on the extent of adsorption was investigated. The experimental data were analyzed by four isotherms and kinetics equations, and the results were fitted well with the Temkin isotherm and pseudo-second-order model. The maximum adsorption capacities (Q_m) of ITG-g-PAO as obtained from Langmuir adsorption isotherm were found to be 100.0, 76.92, 71.42 and 66.67 (mg g^{-1}) for the adsorption of metal ions in order of Co(II) > Zn(II) > Cr(III) > Cd(II). The experimental results demonstrate that the above selective order of adsorption capacity is due to formation of stable chelating ring between the bidentate amidoxime ligand and metal ion.

1. Introduction

Heavy metals unlike organic wastes are non-biodegradable and non-decomposable and they have been excessively released into the environment due to rapid industrialization. Because of their toxic nature, reliable methods are needed to detect and remove heavy metals from environmental samples. Through the traditional methods (Bessbousse, Verchère, & Lebrun, 2012; Fu & Wang, 2011), adsorption process has been found to be more effective and economic in removing heavy metals from aqueous solutions and has attracted considerable attention because of its flexibility and simplicity in design and operation (Afkhami, Saber-Tehrani, & Bagheri, 2010; Murugesan et al., 2011; Sirianuntapiboon & Hongsrisuwan, 2007). Materials of biological origin such as plant wastes or seafood by-products are such abundant renewable sources that have found widespread use for the removal of heavy metal ions from different waste waters due to their relative safety, low cost, free availability and simple technique-needing (Kołodyńska, 2011; Xiao, Tan, & Xue, 2010; Zhu et al., 2011). One of the abundant natural polysaccharide is Iranian tragacanth gum (ITG), a dried, odorless exudation obtained from the stems and branches of *Astragalus gummifer*, specially found in desert highlands of northern and western Iran. ITG is used as a stabilizer and thickening agent in foods and drinks and a binding agent in pharmaceutical products (Meer, Meer, & Gerard, 1973). A comparison between chemically modified and unmodified plant waste adsorbents indicated that the modified ones exhibit higher adsorption capacities (Wan Ngah & Hanafiah, 2008). Adsorbents containing nitrogen such as amine, hydrazine, thioamide, and imidazoline groups have been recently found to be more effective for the removal of cationic metal ions in water (Haratake, Yasumoto, Ono, Akashi, & Nakayama, 2006; Kara, Uzun, Besirli, & Denizli, 2004; Niu, Deng, Yu, & Huang, 2010). The chelating resins with amidoxime functionality (—C—(NH_2)═NOH) are frequently studied because of their unique adsorption properties toward heavy metals (Anirudhan & Ramachandran, 2008; Gao, Gao, & Li, 2010; Horzum, Shahwan, Parlak, & Demir, 2012). Among the techniques of natural polymer modification, graft copolymerization of vinyl monomers, especially acrylonitrile (AN) due to its highest grafting efficiency and also subsequent alkaline hydrolysis is a unique method and has been the subject of extensive investigation (Athawale & Lele, 2000; Ingole & Patil, 2013). Among the variety of adsorbents modified with amidoxime functional groups, no reports are available on the incorporation of ITG with amidoxime functionality yet. Due to low utilization of ITG and its large availability, an attempt was made to obtain ITG incorporated with amidoxime functional groups (ITG-g-PAO) as a new effective biosorbent for

* Corresponding author. Tel.: +98 112 5342350; fax: +98 112 5342350.
E-mail address: ghaemy@umz.ac.ir (M. Ghaemy).

http://dx.doi.org/10.1016/j.carbpol.2014.02.083
0144-8617/

the removal of metal ions in aqueous solution. The prepared adsorbent was characterized by Fourier transform infrared spectroscopy (FTIR), elemental analysis CHNS, atomic force microscopy (AFM), field emission scanning electron microscopy (FESEM), differential scanning calorimeter (DSC) and thermogravimetric analysis (TGA). The basic objectives of the study include; (1) to study the adsorption characteristics of Co(II), Cr(III), Zn(II) and Cd(II) on the modified ITG under equilibrium conditions, (2) to understand the kinetics and (3) to model the adsorption process. For this purpose, batch experiments were conducted and the effect of various factors affecting the adsorption process, such as time of contact, initial pH of the solution, adsorbent dose and metal ion concentration were investigated. The experimental data were fitted to Langmuir, Freundlich, Redlich–Peterson, and Temkin isotherm models. The results were also analyzed on the basis of pseudo-first order, pseudo-second order, Elovich, and Weber–Morris intraparticle diffusion models.

2. Materials and methods

2.1. Chemicals and reagents

The high quality ITG was purchased from local pharmaceutical shop. ITG is a carbohydrate biopolymer with a high molecular weight. Its composition has not yet been fully investigated, but the part soluble in water appears to be a complex mixture of acidic branched hetero-polysaccharides containing d-galacturonic acid. Ceric ammonium nitrate, sodium dodecyl sulfate, hydroxylamine hydrochloride, sodium hydroxide and N,N-dimethylformamide were purchased from Fluka (Darmstadt, Germany) and used without further purification. Acrylonitrile monomer (Fluka, Darmstadt, Germany) was distilled before use. $Cr(NO_3)_3{\cdot}9H_2O$, $Co(NO_3)_2{\cdot}6H_2O$, $Zn(NO_3)_2{\cdot}4H_2O$ and $Cd(NO_3)_2{\cdot}4H_2O$ (1000 mg L^{-1}) standard solutions were used as the sources for Cr(III), Co(II), Zn(II) and Cd(II), respectively. Distilled water (<1microsiemens [μS]) was used for dilution of the stock solutions. pH adjustments were performed with 0.01–1.0 mol L^{-1} HNO_3 and NaOH solutions.

2.2. Methods of characterization

The samples were initially dried in air at 25 °C for 2 days before being analyzed and their surface morphology was examined using field emission scanning electron microscopy (FESEM) (Model: Hitachi S4160). A fragment of the dried sample was mounted on a SEM sample panel and was coated with gold for 2 min. The sample was then mounted in a scanning electron microscope and its surface was scanned at the desired magnification. A PHS-3C pH-meter (Shanghai, Tianyou) was used for pH measurements. The concentration of metal ions in the solution was measured by use of a flame atomic absorption spectrophotometer (Hewlett-Packard 3510) (AAS). In order to determine the mass fraction of carbon, hydrogen and nitrogen, the samples were subjected to elemental analysis using ECS 4010 NCHS Analyzer. FT-IR analysis was carried out on a Bruker Tensor 27 spectrometer (Bruker, karlsrohe, Germany). Polymer samples were prepared by dispersing in dry KBr pellets and recorded between 4000 and 400 cm^{-1}. Atomic force microscopic (AFM) Easy Scan 2 Flex AFM (Swiss Co.) was also used to investigate the surface phase and topography of the sample before and after the sorption process. Differential scanning calorimetry (DSC) thermograms were recorded with a PerkinElmer Pyris 6 under N_2 (20 cm^3 min^{-1}) at a heating rate of 10 °C min^{-1} to measure glass transition temperature (T_g). Thermogravimetric analysis was performed with DuPont Instruments (TGA 951) analyzer at 10 °C min^{-1} heating rate under nitrogen atmosphere in the temperature range of 30–500 °C to determine dynamic weight loss.

2.3. Preparation of polyamidoxime-g-tragacanth adsorbent (ITG-g-PAO)

ITG was sieved to remove dust and small particles, purified with ethanol extraction and then dried under vacuum for 48 h and kept in desiccators before use. The graft polymerization of AN onto ITG was carried out in the presence of ceric ammonium nitrate as an initiator based on the method described previously (Mohamadnia, Zohuriaan-Mehr, Kabiri, & Razavi-Nour, 2008). 1.25 g of dried ITG was dispersed in 125 mL of distilled water in a 500 mL three-necked flask and stirred for 1 h to attain homogenous mixture. 3.32 g (0.062 mol) AN was added into the flask and the mixture was degassed for 20 min under nitrogen atmosphere. The initiator solution (0.46 g ceric ammonium nitrate, 8.39×10^{-4} mol, was dissolved in 4.6 g of 1 N HNO_3) and added to the mixture and stirred at 50 °C for 2 h. A continuous supply of nitrogen was maintained throughout the reaction period. Finally, a few droplets of a 10% aqueous NaOH solution were added to neutralize the mixture which was then poured in methanol to complete precipitation. After filtration, the solid product was stirred gently in DMF for 24 h to remove any polyacrylonitrile (PAN) homopolymer. After centrifugation and decanting the supernatant (PAN in DMF), the tragacanth-g-PAN copolymer (ITG-g-PAN) was precipitated in methanol, thoroughly washed with methanol, and dried at 60 °C to reach a constant weight. In order to obtain the tragacanth graft copolymer with amidoxime functional groups (ITG-g-PAO), the nitrile groups of the grafted copolymer (ITG-g-PAN) were converted to amidoxime groups by using hydroxylamine hydrochloride in aqueous solution. In a 250 mL three-necked flask equipped with a condenser and a magnet stirrer, 0.25 g sodium dodecyl sulfate was dissolved in 30 mL distilled water and stirred for 15 min. 0.5 g ITG-g-PAN was added to this solution and stirred in an ultrasonic water bath for 30 min. A solution of $NH_2OH{\cdot}HCl$ and NaOH (1:1, mole ratio) in 50 mL distilled water (pH 6.5) was added to the mixture and refluxed for 3 h. The solid product, after separation with centrifugation, was washed several times with distilled water to remove the remaining salts and dried in a vacuum oven at 60 °C.

2.4. Adsorption experiments

Adsorption of heavy-metal ions by the prepared modified gum (ITG-g-PAO) from aqueous solutions was investigated in batch experiments. Effects of the initial metal ion concentration, pH of the medium, adsorbent dosage and contact time on the chelation rate and capacity were studied. 25 mL aliquots of aqueous solutions containing different amounts of heavy metal ions (in the range of 20–100 mg L^{-1}), at different pH of the medium (from 2 to 8), with different adsorbent dosage (5–30 mg) and different contact time (from 0 to 100 min) were treated with the chelating beads. The solutions were brought to the desired pH by adding sodium hydroxide (NaOH) and nitric acid (HNO_3), stirred magnetically at 250 rpm and at 25 °C. The pH was maintained in a range of ±0.1 units equilibrium was attained. The concentration of metal ion was analyzed by using a AAS. The instrument response was periodically checked with known heavy metal solution standards. The experiments were performed in replicates of three and the samples were analyzed in replicates of three as well. The following Eq. (1) was used for calculating the removal efficiency of the metal ions:

$$\text{Removal efficiency}(\%) = \left(\frac{C_0 - C_e}{C_0}\right) \times 100 \quad (1)$$

where C_0 and C_e are the initial and the equilibrium ion concentrations (mg L^{-1}), respectively. The adsorption capacity at

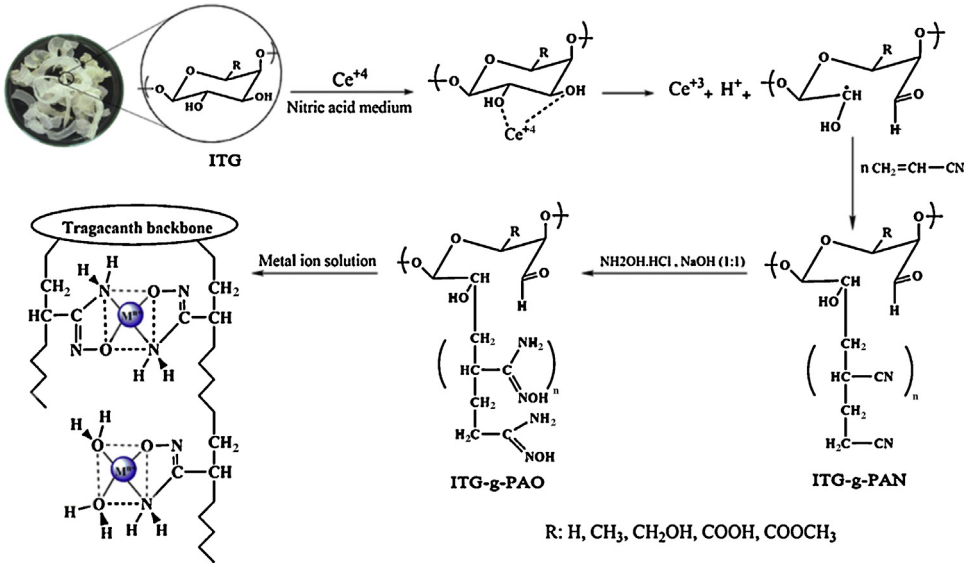

Fig. 1. Illustration of synthetic procedure for preparation of ITG-g-PAO and mechanism of metal ion adsorption.

equilibrium, Q_e (mg g^{-1}), was calculated according to the following formula (2):

$$Q_e = \frac{(C_0 - C_e)}{m} V \quad (2)$$

where V is the volume of the aqueous phase (L); and m is the mass of the adsorbate (mg).

3. Results and discussion

3.1. Preparation and characterization of ITG-g-PAO adsorbent

The use of ceric ammonium nitrate for the chemical initiation of vinyl polymerization has been reported as part of the possible modification of biopolymers, namely, chitin (Ren & Tokura, 1994), starch (Athawale & Lele, 2000), cellulose (Gurdag, Yasar, & Gurkaynak, 1997) and guar gum (Deshmukh & Singh, 1987). Fig. 1 illustrates the entire chemical process of ITG-g-PAO preparation. As shown in this figure, the saccharide ring of gum may be opened when the initiator is multivalent metal ion such as Ce^{4+} ion. It was suggested that there are also other sites such as C6 where this reaction and radical formation can also occur (Gurdag et al., 1997; Mino & Kaizerman, 1958). The metal ion can interact with the C2–C3 glycol of saccharide ring to form a gum–Ce^{4+} complex. The Ce^{4+} ion in the complex can then be reduced as Ce^{3+} ion with the release of a proton and a subsequent formation of a free radical on the backbone of gum. These free radicals could then react with the end vinyl groups of monomer to initiate graft copolymerization (Pottenger & Johnson, 1970; Sharma, Kumar, & Soni, 2003). In this system, the pH of reaction system is important to the initiation efficiency of Ce^{4+} ion. Compared with other initiators such as persulfate and other transition metal ions (i.e., Fe^{3+}, Cu^{2+}, Co^{3+}, Cr^{6+}), the Ce^{3+} initiators usually have higher grafting efficiency and produces a minimum amount of homopolymer (Chowdhury & Pal, 1999). The nitrile groups were converted to amidoxime groups by using hydroxylamine hydrochloride in sodium hydroxide solution. According to Fig. 1, C≡N groups are expected to be replaced with H_2N–C═NOH groups at the end of the reaction. Fig. 2(a) shows FT-IR spectra of ITG, ITG-g-PAN and ITG-g-PAO with changes that are expected during functionalization reaction. FT-IR spectrum of ITG shows characteristic absorption bands at 3448 cm^{-1}, at 1750 and at1660 cm^{-1} which are related to the hydroxyl groups (—OH) and C═O group, respectively. After grafting acrylonitrile to the backbone of ITG, the FT-IR spectrum of ITG-g-PAN in Fig. 2(a) shows the characteristic absorption band of C≡N group at 2240 cm^{-1}. Also, bands at 3400–3200 cm^{-1} and 2950–2860 cm^{-1} correspond to O—H, N—H and C—H stretching's, respectively. After the amidoximation, C≡N bands of 2240 cm^{-1} disappeared and new bands at 1660 cm^{-1} and 926 cm^{-1} corresponding to the stretching vibration of C═N and N—OH bonds, respectively, are formed. These observations clearly indicate the disappearance of original nitrile groups and formation of amidoxime groups effectively, through the treatment with hydroxylamine under specified reaction conditions. Furthermore, the stretching vibration absorption band of —NH_2 group of amidoxime unit at 3300 cm^{-1} overlaps with the absorption band of —OH in the main chain. In order to evaluate the degree of amidoximation incorporation, the synthesized ITG-g-PAO beads were subjected to elemental analysis. The elemental analysis results showed C (36.97%) and H (6.39%) for ITG and C (38.77%), H (6.18%) and N (20.18%) for ITG-g-PAO (Fig. 1S, supplementary figure). This result which has been obtained from a purified ITG-g-PAO sample, from any possible PAN homopolymer, can also support the presence of 20.18% nitrogen atom in the structure of ITG-g-PAO. Thermal properties of the samples were evaluated by DSC and TGA measurements with a heating rate of 10 °C min^{-1} under nitrogen. The glass-transition temperature values (T_gs) were 262 °C, 315 °C and 266 °C for ITG, ITG-g-PAN and ITG-g-PAO, respectively. These changes in the T_g values are related to the polarity of the functional groups in the macromolecule chains.

According to TGA results, the temperatures of 10% weight loss (T_{10}) were 240 °C, 260 °C and 160 °C for ITG, ITG-g-PAN and ITG-g-PAO, respectively. In addition, the amount of carbonized residue (char yield) for ITG-g-PAO in nitrogen atmosphere was up to 40% at 600 °C, implying that the synthesized ITG-g-PAO possess good thermal stability. The solubility behavior of ITG, ITG-g-PAN and ITG-g-PAO was determined at concentration of 5% (w/v) in a number of solvents and the results are shown in Fig. 2(b). As can be seen in this figure, ITG formed a colloidal solution in water while precipitated in THF and chloroform. The graft copolymer of ITG-g-PAN precipitated in water and THF and floated in chloroform while after reduction of C≡N groups, ITG-g-PAO precipitated in water and THF and formed a dispersed solution in chloroform.

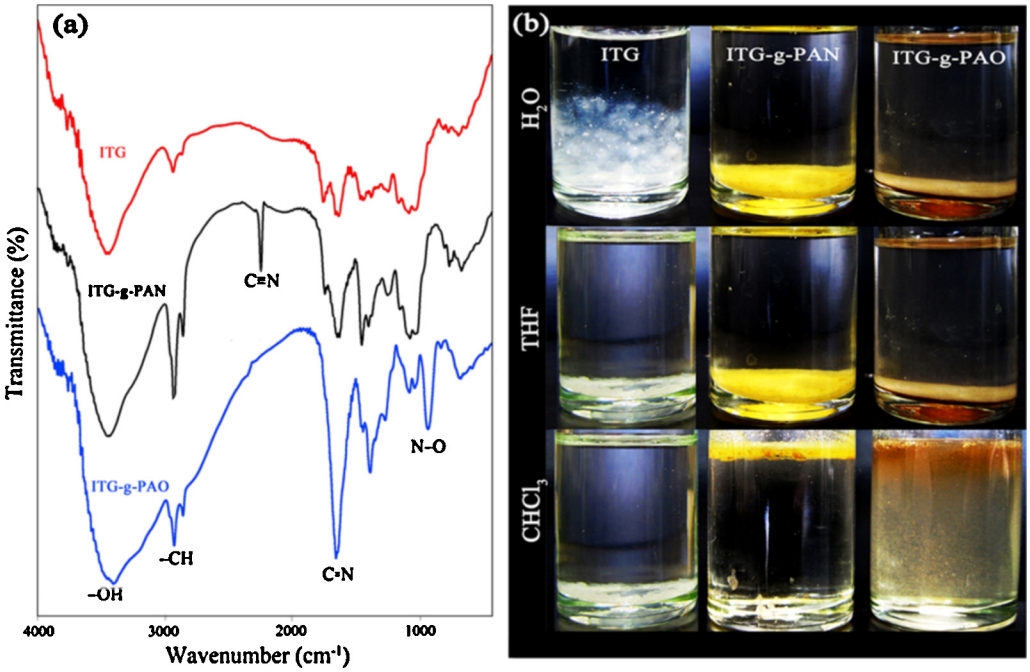

Fig. 2. (a) FT-IR spectra of ITG, ITG-g-PAN, and ITG-g-PAO, and (b) their solubility behavior in water, THF and chloroform.

Fig. 3(a) shows SEM images of the top view of ITG, ITG-g-PAN and ITG-g-PAO. As can be seen in these images, the apparent morphology of the amidoximated graft copolymer (ITG-g-PAO) is completely different from the morphology of ITG-g-PAN after reaction with the hydroxylamine hydrochloride. As shown in SEM image in Fig. 3(a), the particles size for ITG-g-PAO is in the range of nanoscale (40–60 nm). Fig. 3(b) shows 3D AFM images of the top view of ITG-g-PAO before and after metal ion adsorption. As can be seen in the image after adsorption, the surface is fully covered with layer of absorbed substance which is revealed by many peaks and valleys on the surface. The AFM histogram of size distribution, in Fig. 3(b), also shows the average size for ITG-g-PAO particles in the range of 10–45 nm before metal ion adsorption. The size of ITG-g-PAO particles increased to a very wide range with the average size of 65–85 nm after metal ion adsorption.

3.2. Adsorption properties of the ITG-g-PAO for metal ions

3.2.1. Effect of solution pH

The amidoximes exist predominantly in the syn-hydroxyamino form that is stabilized by an intramolecular hydrogen bond and in water these compounds behave as bases. Therefore, pH of the aqueous solution is an important parameter in the adsorption process. Experiments were performed in the pH range of 2.0–8.0, where chemical precipitation is avoided, so that removal could be related to the adsorption process. The 25 mL suspension (initial concentration: 20 mg L^{-1}) was stirred by a magnet for 60 min at 25 °C. After centrifugal separation, the metal ion concentrations in the supernatants were determined by AAS.

Fig. 4(a) shows the effect of pH on the adsorption of metal ions onto ITG-g-PAO. At low pH, the active sites of the adsorbent are less available for metal ions due to protonation of the above sites at higher H^+ concentration. Therefore, the adsorption capacities increased with increasing pH, reaching plateau values around pH 6.0 for all metals. Higher adsorption at higher pH values may imply that metal ions interact with adsorbent by a chelating mechanism. At this optimum pH, the removal efficiencies for Cd(II), Cr(III), Co(II), and Zn(II) ions were 56.65%, 78.25%, 83.85%, and 66.20%, respectively.

3.2.2. Effect of adsorbent dosage

The effect of ITG-g-PAO dosage on the amount of the tested metal ions adsorbed was studied by contacting 25 mL of each metal ion solution (20 mg L^{-1}: initial concentration) with different amounts of adsorbent (5–30 mg L^{-1}) at pH = 6 for 60 min at 25 °C. The suspensions were centrifuged and the supernatants were analyzed by AAS. The result in Fig. 4(b) shows that increase in adsorption was sharp with the increase in the adsorbent dosage and reached to the maximum values of 56.65%, 78.25%, 83.85% and 66.20% for Cd(II), Cr(III), Co(II), and Zn(II) ions, respectively when the amount of adsorbent increased from 5 to 20 mg L^{-1}. However, saturation occurred at 20 mg adsorbent at which further increase in dosage caused gradual increase on ion adsorption. This can probably suggest that adsorption of metal ions occurs mostly with active sites on the surface of sample.

3.2.3. Effect of contact time

To identify the rapidness of binding and removal processes of the tested metal ions by the newly modified adsorbent, the effect of contact time on metal ion adsorption at the other optimum conditions was investigated. Therefore, to determine the equilibrium time for the maximum removal efficiency, 25 mL of each metal ion solution (initial concentration = 20 mg L^{-1}) containing 0.2 g ITG-g-PAO at pH = 6 was stirred from 0 to 100 min. Fig. 4(c) shows the adsorption capacities of the tested metal ions against contact time. The rapid adsorption of metal ions pending the first 15 min can be due to the larger surface area of ITG-g-PAO nanohydrogel and the abundant accessibility of active sites [—$C(NH_2)$=NOH] on the adsorbent surface. After that, adsorption slowed down and the equilibrium was attained at 60 min for all tested metals. The experimental values of adsorption capacity of ITG-g-PAO for metal ions at the equilibrium were 14.16, 19.56, 20.96, and 16.55 (mg g^{-1}) for Cd(II), Cr(III), Co(II), and Zn(II) ions, respectively, as shown in Fig. 4(c). Since the equilibrium concentration was not seriously

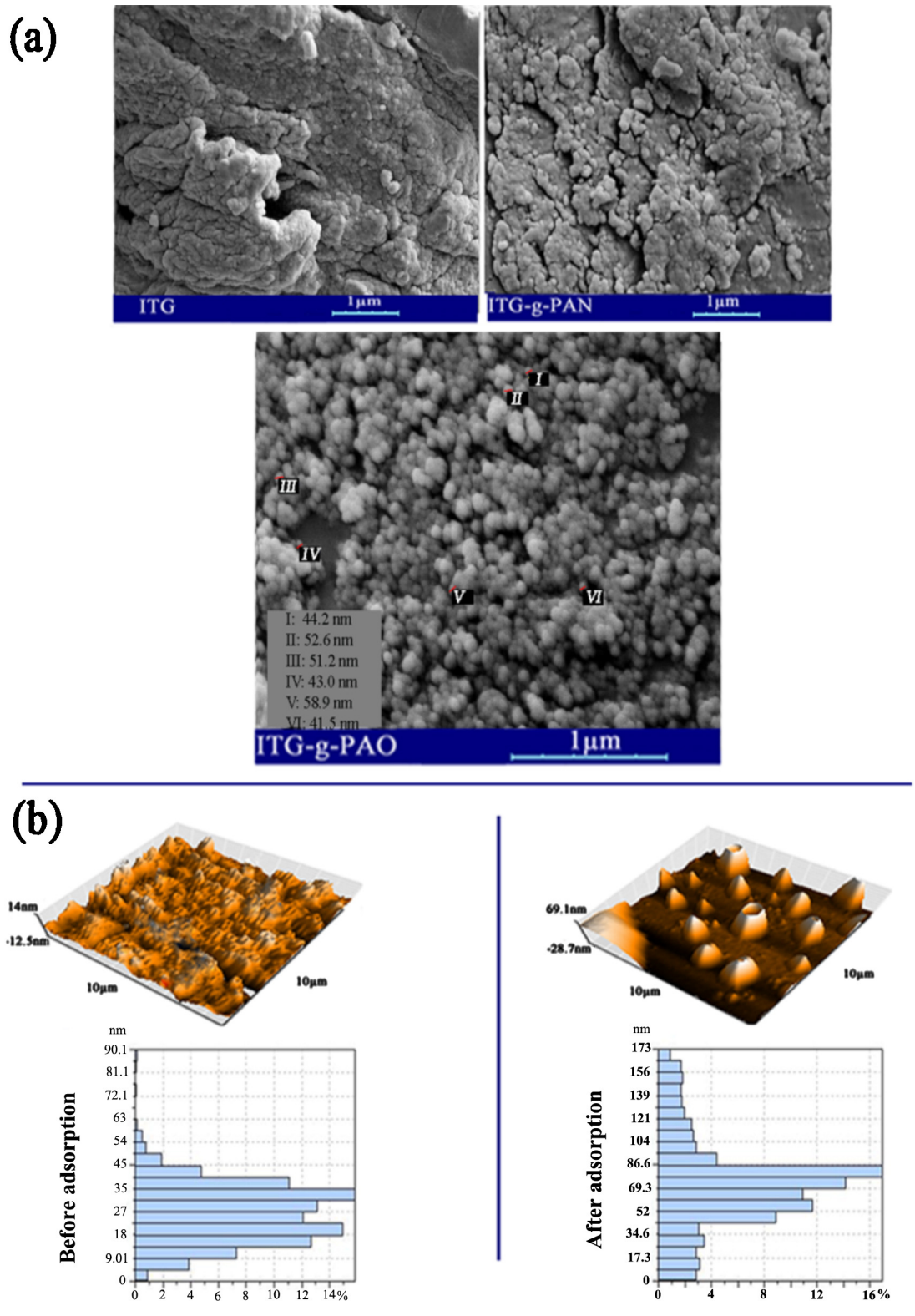

Fig. 3. (a) FESEM images of ITG, ITG-g-PAN and ITG-g-PAO, and (b) AFM images of ITG-g-PAO before and after adsorption of Cd^{2+}.

influenced by the more retention time, the optimum contact time was considered to be 60 min.

3.2.4. *Effect of initial metal ion concentration*

To investigate the effect of initial concentration of metal ions (from 20 mg L^{-1} to 100 mg L^{-1}) on the adsorption and isotherm studies, batch experiments were performed at 25 °C with optimum dosage of adsorbent, time, and pH. Sorption capacity (mg g^{-1}) or the efficiency (%) of an adsorbent is the maximum amount of metal ion removed from the solution when the chelating sites of the sorbent are saturated. Fig. 4(d) shows the efficiency of the ITG-g-PAO to remove the metal ions from aqueous solutions with different initial feed solution concentrations varying from 20 to 100 mg L^{-1}. The figure shows that the efficiency of the adsorbent is dependent on

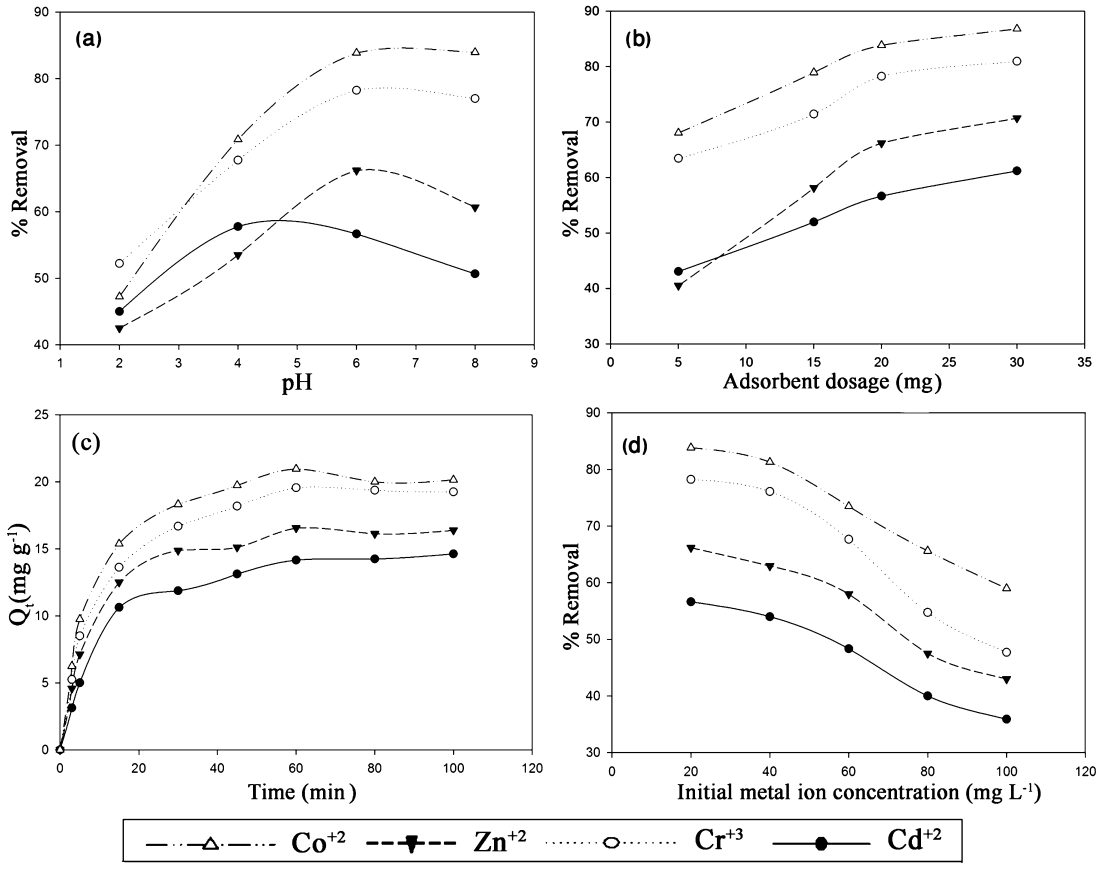

Fig. 4. Effect of pH (a), adsorbent dosage (b), contact time (c) and initial metal ion concentration (d) on the adsorption.

the initial feed solution concentration as well as the metal ion itself. For all the investigated metal ions, the efficiency of the ITG-g-PAO copolymer hydrogel decreased 20–30% by increasing the feed solution concentration. At higher initial concentration the total existing adsorption sites were confined; thus, resulting in a decrease of metal ions removal efficiency. According to these results the prepared hydrogel possessed high efficiency in the range of up to 40 mg L^{-1} that it removes about 55–83% of the tested metal ions from aqueous solution.

3.2.5. Sorption isotherm models

The adsorption isotherms describe the effect of different initial metal ion concentrations on the amount of metal ion adsorbed on the adsorbent surface, leading to find the best equilibrium position in the adsorption process. There are different equilibrium isotherm equations proposed in literature. In the present study, the adsorption isotherms were investigated by the Langmuir, Freundlich, Redlich–Peterson, and Temkin equations.

3.2.5.1. The Freundlich isotherm. The Freundlich isotherm model is the earliest empirical equation based on the adsorption on reversible heterogeneous surfaces. The mathematical expression of the model is given as follows (Shen et al., 2009):

$$\ln Q_e = \ln K_f + \frac{1}{n} \ln C_e \quad (3)$$

where K_f is a constant related to the adsorption capacity and $1/n$ is an empirical parameter related to the adsorption intensity, which varies with the heterogeneity of material, determines the affinity of the process to be a chemisorptions ($n < 1$) or a physisorption ($n > 1$). Q_e and C_e are the equilibrium adsorption capacity (mg g^{-1}) and the equilibrium concentration (mg L^{-1}), respectively. By using the linear Freundlich isotherm equation, the isotherm constants were predicted from the plot between $\ln Q_e$ and $\ln C_e$ and the results are tabulated in Table 1.

3.2.5.2. The Langmuir isotherm. The theoretical Langmuir isotherm model is often used to describe the equilibrium adsorption isotherms of homogeneous surfaces (Shin, Hong, & Jang, 2011). This isotherm model assumes that all sites possess equal affinity for the adsorbate (Foo & Hameed, 2010). In this theory, the adsorption reaches to its maximum level after a complete monolayer formation of adsorbate molecules onto the adsorbent surface (Murugesan et al., 2011). Mathematically, the equation can be written as follows:

$$\frac{C_e}{Q_e} = \frac{1}{Q_m K_L} + \frac{C_e}{Q_m} \quad (4)$$

where Q_m is the maximum metal ion uptake capacity (mg g^{-1}), K_L is the Langmuir constant related to the adsorption energy (L mg^{-1}), and Q_e and C_e are defined as previous. By using the linear Langmuir isotherm equation, the isotherm constants were calculated from the plot between C_e/Q_e and C_e and the results are tabulated in Table 1.

3.2.5.3. The Temkin isotherm. The Temkin isotherm model is based on two assumptions: (i) heat of adsorption would decrease linearly rather than logarithmic with the coverage, and (ii) its derivation is characterized by a uniform distribution of binding energies up to some maximum binding energy (Dada, Olalekan, Olatunya, & DADA, 2012). The Temkin isotherm equation would be:

$$Q_e = B \ln(AC_e) \quad (5)$$

Table 1
Isotherm and kinetic models and their statistical parameters at 25 °C and at pH 6.0.

Isotherm & kinetic models	Parameters	Metal ions			
		Co^{2+}	Cr^{3+}	Zn^{2+}	Cd^{2+}
Langmuir	Q_m (mg g^{-1})	100	71.428	76.923	66.667
	K_L (L mg^{-1})	0.0884	0.106	0.046	0.035
	R^2	0.9647	0.9759	0.9750	0.9833
Freundlich	K_f ((mg g^{-1})(L mg^{-1})$^{(1/n)}$)	13.423	12.353	6.612	4.645
	n	2.079	2.352	1.855	1.769
	R^2	0.9462	0.8574	0.9139	0.9267
Redlich–Peterson	K_R (L g^{-1})	−35.71	−17.85	−13.698	−10.2
	α_R (L mg^{-1})	−2.928	−1.642	−2.315	−2.438
	β	0.518	0.574	0.46	0.434
	R^2	0.9543	0.8606	0.9271	0.9392
Temkin	A (L g^{-1})	0.9039	0.9966	0.4139	0.31
	B	20.53	15.66	17.21	15.18
	R^2	0.9979	0.9561	0.9833	0.99
Pseudo-first-order	K_1 (min^{-1})	0.0598	0.0575	0.0575	0.0575
	$Q_{e,\,cal.}$ (mg g^{-1})	16.982	16.865	13.458	12.647
	R^2	0.9809	0.9826	0.9198	0.9588
Pseudo-second-order	K_2 (g mg^{-1} min^{-1})	1.09×10^{-2}	6.67×10^{-3}	7.396×10^{-3}	4.18×10^{-3}
	$Q_{e,\,cal.}$ (mg g^{-1})	21.276	21.276	17.857	16.95
	$Q_{e,\,exp.}$ (mg g^{-1})	20.9625	19.5625	16.55	14.1625
	R^2	0.9956	0.9934	0.9934	0.9803
Elovich equation	α (mg g^{-1} min^{-1})	8.72	6.228	5.867	3.413
	β (g mg^{-1})	0.243	0.24	0.289	0.298
	R^2	0.9453	0.9705	0.9494	0.9692
Intraparticle diffusion	K_p (mg g^{-1} min$^{-1/2}$)	1.99	1.95	1.628	1.505
	C	4.175	3.248	3.022	1.83
	R^2	0.8449	0.8841	0.8563	0.8956

where $B = RT/b$ and A (L mg^{-1}) is Temkin constant representing the equilibrium binding. The mentioned isotherm constants were calculated from the plot between Q_e and ln C_e and the results are listed in Table 1.

3.2.5.4. The Redlich–Peterson isotherm. The Redlich–Peterson isotherm model is used to incorporate features of both the Langmuir and Freundlich model equations. At low concentrations the Redlich–Peterson isotherm approximates to Langmuir model and at high concentrations it approaches the Freundlich model isotherm (Murugesan et al., 2011). The linear and non-linear equation forms are given as:

$$\frac{C_e}{Q_e} = \frac{1}{K_R} + \frac{\alpha_R}{K_R} C_e^{\beta} \tag{6}$$

where K_R (L g^{-1}), α_R (L mg^{-1}), and β are Redlich–Peterson isotherm constants. The constant β lies between 0 and 1 and determines whether the Langmuir isotherm ($\beta = 1$), or the Freundlich isotherm ($\beta = 0$) is preferred. Since there are three unknown constants presented in the linear form equation (α_R, K_R, β), the determination process would need one more step and it would be the use of a plot between ln C_e/Q_e and ln C_e (secondary linear form), the results are tabulated in Table 1.

The experimental adsorption data for ITG-g-PAO that were affected by the change of initial metal ion concentrations, as compared in Fig. 2S (supplementary figure), were fitted to the isotherm equations and the graphical results are presented in Fig. 5. According to the figures, the Q_e value keeps increasing with the increase of metal ions concentration. Table 1 shows the calculated constants of the above isotherm equations. By comparing the R^2 values of these isotherms for the tested metal ions, we can find the most respective and suitable equation for fitting the experimental data. As it is presented in Table 1 and shown in Fig. 5, the nearest R^2 values to 1 belong to the Temkin equation and this indicates that the respective equation fits with the experimental data best. Also, the Langmuir isotherm equation has a good conformity with experimental data and the Q_m values of ITG-g-PAO obtained by this equation are compared with other adsorbents found from literature (Table 2). According to Table 2, the adsorption capacity of ITG-g-PAO is much higher than almost all of the reported adsorbents and this indicates that ITG-g-PAO can be a good candidate for the applications related to heavy metal ion removal.

3.2.6. Adsorption kinetics

The adsorption kinetics process was investigated by four kinetic models: Lagergren pseudo-first-order, pseudo-second-order, Elovich equation, and intraparticle diffusion. Parameters of the kinetic models and coefficients of determination (R^2) were calculated to determine the conformity of the models with the experimental data; the results are presented in Table 1. Fig. 6 shows the linear plots of the kinetic models for all the tested metal ions.

3.2.6.1. Lagergren pseudo-first-order kinetic model. This model is based on the assumption that the adsorption rate relates to the number of the unoccupied adsorptive sites, and is expressed as follows (Monier, Ayad, & Sarhan, 2010):

$$\log(Q_e - Q_t) = \log Q_e - \frac{k_1}{2.303} t \tag{7}$$

where Q_t and Q_e (mg g^{-1}) are the adsorption capacities at time t and equilibrium, respectively, and k_1 (min^{-1}) is the pseudo-first-order rate constant. The slopes of linear plots of log($Q_e - Q_t$) versus t, Fig. 6(a), give k_1 values listed in Table 1. Accordingly, the pseudo-first-order model has a good fit with the experimental data.

3.2.6.2. The pseudo-second-order kinetic model. The pseudo-second-order kinetic model notes that the adsorption should relate to the squared product of the difference between the number of the equilibrium adsorptive sites available on an adsorbent and that of the occupied sites. This model is expressed as follows (Monier et al., 2010):

$$\frac{t}{Q_t} = \frac{1}{k_2 Q_e^2} + \frac{1}{Q_e} t \tag{8}$$

where k_2 is the pseudo-second-order rate constant (g mg^{-1} min^{-1}), and is obtained from the slope of linear plot of t/Q_t versus t, Fig. 6(b)

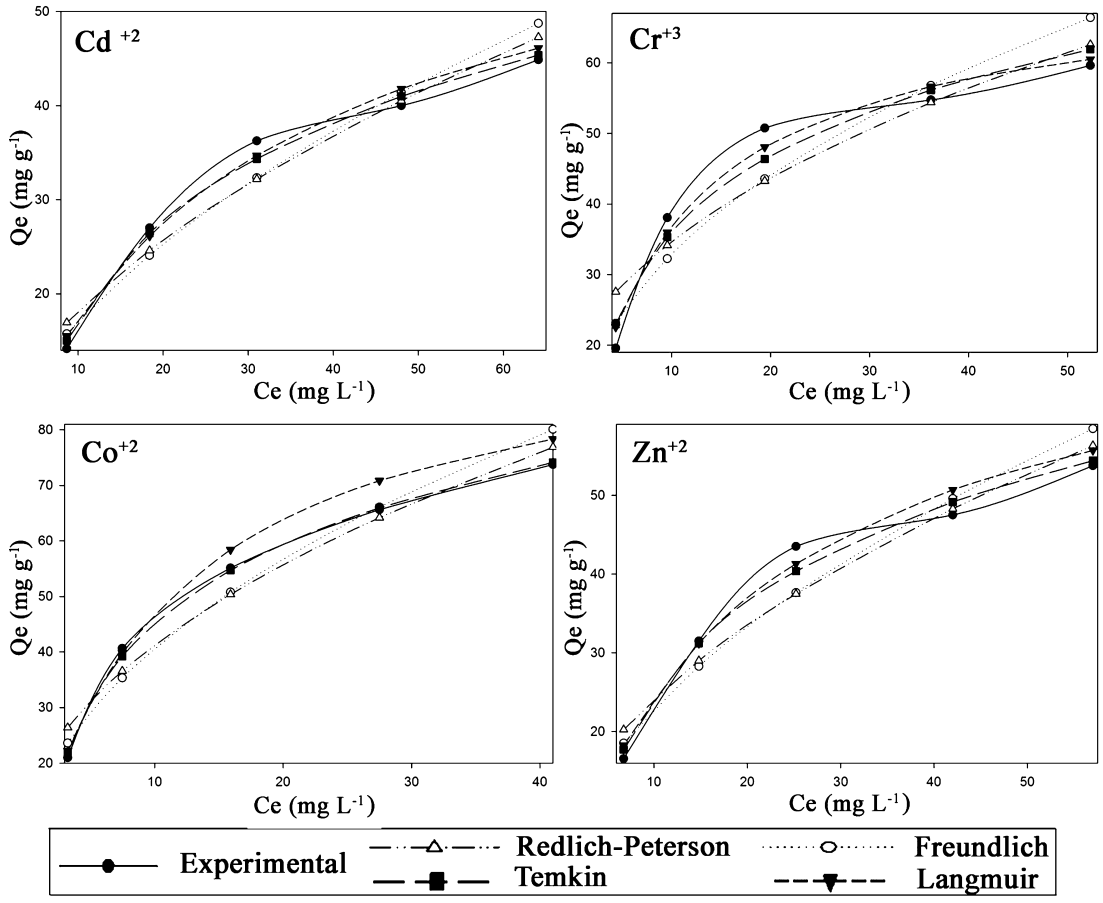

Fig. 5. The adsorption isotherms of ITG-g-PAO for: (a) Cd(II), (b) Cr(III), (c) Co(II), and (d) Zn(II) ions. (Temperature = 25 °C, contact time = 60 min, C_0 = 20–100 mg L^{-1}, adsorbent dosage = 20 mg, pH = 6).

and Table 1. According to the R^2 values, it is clear that this model fits the experimental data best. Also, comparison between the calculated and experimental adsorption capacities ($Q_{e,\,cal.}$ and $Q_{e,\,exp.}$, respectively), admits the high applicability of the pseudo-second-order model to describe the sorption process.

3.2.6.3. The Elovich kinetic model. The linear form of this model is expressed as:

$$Q_t = \frac{1}{\beta}\ln(\alpha\beta) + \frac{1}{\beta}\ln t \tag{9}$$

where α (mg g^{-1} min^{-1}) and β (g mg^{-1}) are the Elovich coefficients, representing the initial sorption rate and the extent of the surface coverage and activation energy, respectively. The Elovich constants could be computed from the plot of Q_t versus $\ln t$, as shown in Fig. 6(c) and in Table 1. According to the results the Elovich kinetics model has a good fit with the experimental results.

3.2.6.4. The Weber–Morris intraparticle diffusion model. This model is expressed as:

$$Q_t = K_p t^{1/2} + C \tag{10}$$

where C and K_p (mg g^{-1} $min^{-1/2}$) are the intercept and the intraparticle diffusion rate constant, respectively. The constants could be found by the linear plot of Q_t versus $t^{1/2}$, as shown in Fig. 6(d) and in Table 1. According to the results, the intraparticle diffusion model shows a poor fit to the experimental data. Based on the coefficient values listed in Table 1, it can be inferred that the

Table 2
Comparison of the maximum adsorption capacity of various adsorbents.

Adsorbent	Maximum adsorption capacity, Q_m (mg g^{-1})				References
	Co^{2+}	Cr^{3+}	Zn^{2+}	Cd^{2+}	
ITG-g-PAO	100	71.42	76.92	66.67	Present work
Un-treated peat moss	30.03	–	–	–	Caramalău, Bulgariu, and Macoveanu (2009)
Bagasse carbon	–	–	–	30	Mohan and Singh (2002)
Sugar beet pulp	–	–	17.7	24.3	Reddad, Gerente, and Andres (2002)
Cassava tuber bark waste	–	–	83.3	26.3	Horsfall, Abia, and Spiff (2006)
Aquatic fern	–	–	48	86	Ganji, Khosravi, and Rakhsaee (2005)
Carrot residues	–	45.09	29.61	–	Nasernejad, Esslam Zadeh, Bonakdar Pour, Esmaail Bygi, and Zamani (2005)
Peanut husk	–	7.67	–	–	Li, Zhai, Zhang, Wang, and Zhou (2006)
Crosslinked chitosan with epichlorohydrin	–	–	10.2	–	Chen, Liu, Chen, and Chen (2008)

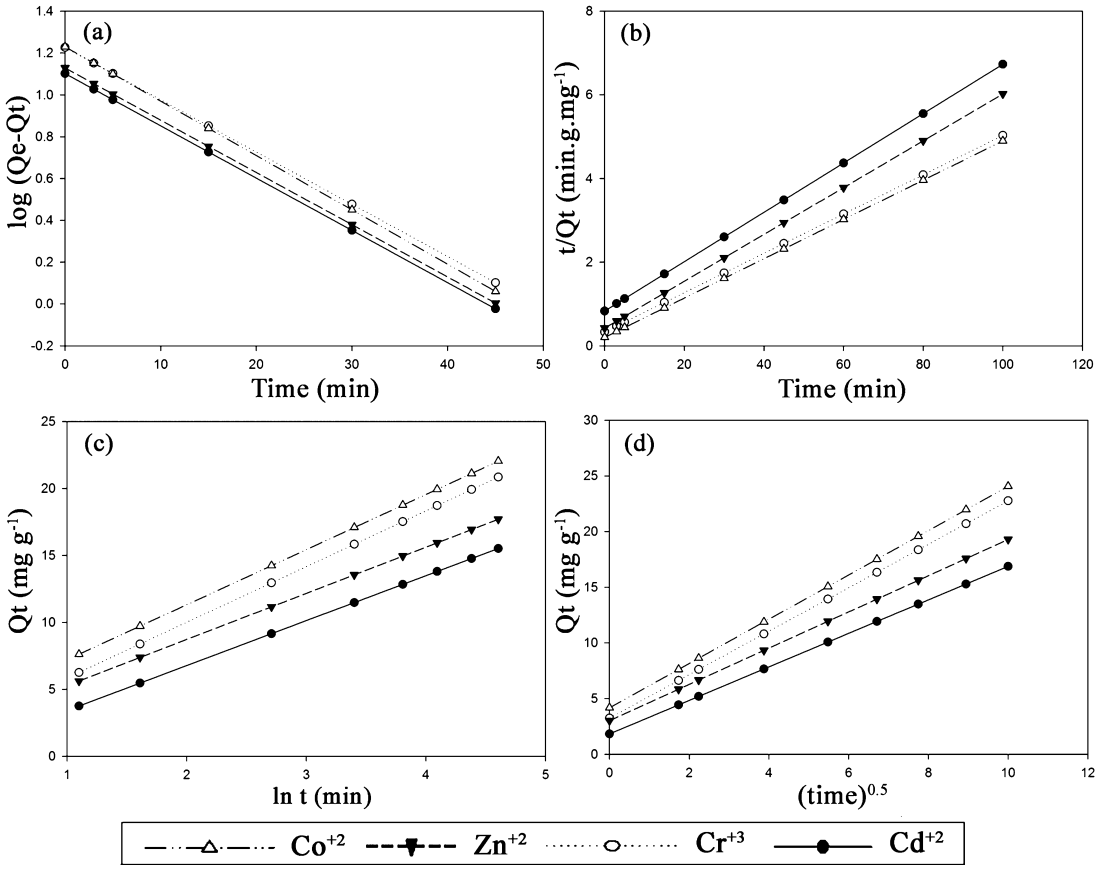

Fig. 6. Kinetic models for the adsorption of Cd(II), Cr(III), Co(II), and Zn(II) ions: (a) pseudo-first-order, (b) pseudo-second-order, (c) Elovich and (d) Weber–Morris intraparticle diffusion model. (Temperature = 25 °C, C_0 = 20 mg L^{-1}, adsorbent dosage = 20 mg, pH = 6).

pseudo-second-order model has the highest conformity with the experimental data.

4. Conclusion

The tragacanth gum-graft-polyamidoxime was synthesized, fully characterized and used as an effective sorbent through metal-amidoxime chelating mechanism for the removal of heavy metals from aqueous solutions. The sorption was solution pH dependent and the highest removal occurred at pH 6.0 in approximately 1 h. It was observed from the experiments that about 57–84% removal is possible at lower concentration ranges (20 mg L^{-1}). Kinetic adsorption data followed pseudo second-order rate expression. The experimental adsorption isotherm data were best fitted with Temkin isotherm model, and the maximum adsorption capacity was found to be 100.0, 76.92, 71.42 and 66.67 (mg g^{-1}) Co(II)> Zn(II) > Cr(III) > Cd(II), respectively.

Appendix A. Supplementary data

Supplementary data associated with this article can be found, in the online version, at http://dx.doi.org/10.1016/j.carbpol.2014.02.083.

References

Afkhami, A., Saber-Tehrani, M., & Bagheri, H. (2010). Simultaneous removal of heavy-metal ions in wastewater samples using nano-alumina modified with 2,4-dinitrophenylhydrazine. *Journal of Hazardous Materials*, *181*, 836–844.

Anirudhan, T. S., & Ramachandran, M. (2008). Synthesis and characterization of amidoximated polyacrylonitrile/organobentonite composite for Cu(II), Zn(II), and Cd(II) adsorption from aqueous solutions and industry wastewaters. *Industrial and Engineering Chemistry Research*, *47*, 6175–6184.

Athawale, V. D., & Lele, V. (2000). Syntheses and characterisation of graft copolymers of maize starch and methacrylonitrile. *Carbohydrate Polymers*, *41*, 407–416.

Bessbousse, H., Verchère, J. F., & Lebrun, L. (2012). Characterisation of metal-complexing membranes prepared by the semi-interpenetrating polymer networks technique. Application to the removal of heavy metal ions from aqueous solutions. *Chemical Engineering Journal*, *187*, 16–28.

Caramalău, C., Bulgariu, L., & Macoveanu, M. (2009). Cobalt (II) removal from aqueous solutions by adsorption on modified peat moss. *Chemical Bulletin of "POLITEHNICA" University of Timisoara*, *54*(68), 13–17.

Chen, A. H., Liu, S. C., Chen, C. Y., & Chen, C. Y. (2008). Comparative adsorption of Cu(II), Zn(II), and Pb(II) ions in aqueous solution on the crosslinked chitosan with epichlorohydrin. *Journal of Hazardous Materials*, *154*, 184–191.

Chowdhury, P., & Pal, C. M. (1999). Graft copolymerization of methyl acrylate onto polyvinyl alcohol using Ce(IV) initiator. *European Polymer Journal*, *35*, 2207–2213.

Dada, A. O., Olalekan, A. P., Olatunya, A. M., & DADA, O. (2012). Langmuir, Freundlich, Temkin and Dubinin–Radushkevich isotherms studies of equilibrium sorption of Zn^{2+} unto phosphoric acid modified rice husk. *Journal of Applied Chemistry*, *3*(1), 38–45.

Deshmukh, S. R., & Singh, R. P. (1987). Drag reduction effectiveness, shear stability and biodegradation resistance of guargum-based graft copolymers. *Journal of Applied Polymer Science*, *33*, 1963–1975.

Foo, K. Y., & Hameed, B. H. (2010). Insights into the modeling of adsorption isotherm systems. *Chemical Engineering Journal*, *156*, 2–10.

Fu, F., & Wang, Q. (2011). Removal of heavy metal ions from wastewaters: A review. *Journal of Environment Management*, *92*, 407–418.

Ganji, M. T., Khosravi, M., & Rakhsaee, R. (2005). Biosorption of Pb, Cd, Cu and Zn from wastewater by treated Azolla filiculoides with H_2O_2/$MgCl_2$. *International Journal of Environmental Science and Technology*, *1*, 265–271.

Gao, B., Gao, Y., & Li, Y. (2010). Preparation and chelation adsorption property of composite chelating material poly(amidoxime)/SiO_2 towards heavy metal ions. *Chemical Engineering Journal*, *158*, 542–549.

Gurdag, G., Yasar, M., & Gurkaynak, M. A. (1997). Graft copolymerization of acrylic acid on cellulose: Reaction kinetics of copolymerization. *Journal of Applied Polymer Science*, *66*, 929–934.

Haratake, M., Yasumoto, K., Ono, M., Akashi, M., & Nakayama, M. (2006). Synthesis of hydrophilic macroporous chelating polymers and their versatility in the preconcentration of metals in seawater samples. *Analytica Chimica Acta*, *561*, 183–190.

Horsfall, M., Jr., Abia, A. A., & Spiff, A. I. (2006). Kinetic studies on the adsorption of Cd^{2+}, Cu^{2+} and Zn^{2+} ions from aqueous solutions by cassava (Manihot sculenta Cranz) tuber bark waste. *Bioresource Technology*, *97*, 283–291.

Horzum, N., Shahwan, T., Parlak, O., & Demir, M. M. (2012). Synthesis of amidoximated polyacrylonitrile fibers and its application for sorption of aqueous uranyl ions under continuous flow. *Chemical Engineering Journal*, *213*, 41–49.

Ingole, N. W., & Patil, V. N. (2013). Cadmium removal from aqueous solution by modified low cost adsorbent(s): A state of the art. *International Journal of Civil, Structural, Environmental and Infrastructure Engineering Research and Development (IJCSEIERD)*, *3*(4), 17–26.

Kara, A., Uzun, L., Besirli, N., & Denizli, A. (2004). Poly(ethylene glycol dimethacrylate-n-vinyl imidazole) beads for heavy metal removal. *Journal of Hazardous Materials*, *106*, 93–99.

Kołodyńska, D. (2011). Chitosan as an effective low-cost sorbent of heavy metal complexes with the polyasparticacid. *Chemical Engineering Journal*, *173*, 520–529.

Li, Q., Zhai, J., Zhang, W., Wang, M., & Zhou, J. (2006). Kinetic studies of adsorption of Pb(II), Cr(III) and Cu(II) from aqueous solution by sawdust and modified peanut husk. *Journal of Hazardous Materials*, *141*, 163–167.

Meer, G., Meer, W. A., & Gerard, T. (1973). In L. Whistler, & J. N. Bemiller (Eds.), *Industrial gums (polysaccharides and their derivatives)* (pp. 289–299). New York: Academic Press.

Mino, G., & Kaizerman, S. (1958). A new method for the preparation of graft copolymers. Polymerization initiated by ceric ion redox systems. *Journal of Polymer Science*, *31*, 242–243.

Mohamadnia, Z., Zohuriaan-Mehr, M. J., Kabiri, K., & Razavi-Nour, M. (2008). Tragacanth gum-graft-polyacrylonitrile: Synthesis, characterization and hydrolysis. *Journal of Polymer Research*, *15*, 173–180.

Mohan, D., & Singh, K. P. (2002). Single- and multi-component adsorption of cadmium and zinc using activated carbon derived from Bagasse—An agricultural waste. *Water Research*, *36*, 2304–2318.

Monier, M., Ayad, D. M., & Sarhan, A. A. (2010). Adsorption of Cu(II), Hg(II), and Ni(II) ions by modified natural wool chelating fibers. *Journal of Hazardous Materials*, *176*, 348–355.

Murugesan, A., Ravikumar, L., SathyaSelvaBala, V., SenthilKumar, P., Vidhyadevi, T., Dinesh Kirupha, S., et al. (2011). Removal of Pb(II), Cu(II) and Cd(II) ions from aqueous solution using polyazomethineamides: Equilibrium and kinetic approach. *Desalination*, *271*, 199–208.

Nasernejad, B., Esslam Zadeh, T., Bonakdar Pour, B., Esmaail Bygi, M., & Zamani, A. (2005). Comparison for biosorption modeling of heavy metals (Cr(III), Cu(II), Zn(II)) adsorption from wastewater by carrot residues. *Process Biochemistry*, *40*, 1319–1322.

Niu, L., Deng, S., Yu, G., & Huang, J. (2010). Efficient removal of Cu(II), Pb(II), Cr(VI) and As(V) from aqueous solution using an aminated resin prepared by surface-initiated atom transfer radical polymerization. *Chemical Engineering Journal*, *165*, 751–757.

Pottenger, C. R., & Johnson, D. C. (1970). Mechanism of cerium (IV) oxidation of glucose and cellulose. *Journal of Polymer Science Part A-1: Polymer Chemistry*, *8*, 301–318.

Reddad, Z., Gerente, C., & Andres, Y. (2002). Adsorption of several metal ions onto a low-cost biosorbent: Kinetic and equilibrium studies. *Environmental Science and Technology*, *36*, 2067–2073.

Ren, L., & Tokura, S. (1994). Structural aspects of poly(methylmethacrylate)-grafted B-chitin copolymers initiated by ceric salts. *Carbohydrate Polymers*, *23*, 19–25.

Sharma, B. R., Kumar, V., & Soni, P. L. (2003). Graft copolymerization of acrylonitrile onto Cassia tora gum with ceric ammonium nitrate–nitric acid as a redox initiator. *Journal of Applied Polymer Science*, *90*, 129–136.

Shen, W., Chen, S., Shi, S., Li, X., Zhang, X., Hu, W., et al. (2009). Adsorption of Cu(II) and Pb(II) onto diethylenetriamine-bacterial cellulose. *Carbohydrate Polymers*, *75*, 110–114.

Shin, K. Y., Hong, J. Y., & Jang, J. (2011). Heavy metal ion adsorption behavior in nitrogen-doped magnetic carbon nanoparticles: Isotherms and kinetic study. *Journal of Hazardous Materials*, *190*, 36–44.

Sirianuntapiboon, S., & Hongsrisuwan, T. (2007). Removal of Zn^{2+} and Cu^{2+} by a sequencing batch reactor (SBR). *Bioresource Technology*, *98*(4), 808–818.

Wan Ngah, W. S., & Hanafiah, M. A. K. M. (2008). Removal of heavy metal ions from wastewater by chemically modified plant wastes as adsorbents: A review. *Bioresource Technology*, *99*, 3935–3948.

Xiao, C. M., Tan, J., & Xue, G. N. (2010). Synthesis and properties of starch-g-poly(maleic anhydride-co-vinyl acetate)? *eXPRESS Polymer Letters*, *4*(1), 9–16.

Zhu, H., Jia, S., Wan, T., Jia, Y., Yang, H., Li, J., et al. (2011). Biosynthesis of spherical Fe_3O_4/bacterial cellulose nanocomposites as adsorbents for heavy metal ions. *Carbohydrate Polymers*, *86*, 1558–1564.